Frequency Diversity MIMO Detection for DP-QAM Transmission

Masaki Sato, Robert Maher, *Member, IEEE*, Domaniç Lavery, *Member, IEEE*, Kai Shi, *Member, IEEE,* Benn C. Thomsen, *Member, IEEE*, and Polina Bayvel, *Fellow, IEEE*

***Abstract*—Dual-carrier 10GBaud DP-16QAM transmission system with frequency diversity multiple-input-multiple-output (FD-MIMO) detection is described. In transmission over 800km of standard single mode fiber (SSMF), with a dual-carrier spacing of 0.8×symbol-rate, a Q^2-factor penalty of only 1.7dB, relative to single carrier performance, is achieved. The performance of FD-MIMO for linear crosstalk mitigation is experimentally demonstrated by varying the channel spacing from 0.4 to 1.2×symbol-rate in a dual-carrier DP-16QAM and DP-QPSK back-to-back configuration. Three channel FD-MIMO equalization for both modulation formats is also studied in the same configuration. In addition, the combination of optical filtering and FD-MIMO, indicates that a guard band of 10% of the symbol-rate is sufficient to avoid additional linear crosstalk from neighboring WDM channels.**

***Index Terms*—Multi channel equalizer, multi-input-multi-output (MIMO), spectral efficiency (SE), coherent, wavelength division multiplexing (WDM), digital signal processing (DSP), quadrature amplitude modulation (QAM), optical transmission.**

I. Introduction

SINCE the commercial deployment of 100G long-haul wavelength division multiplexing (WDM) systems, enabled by optical coherent receivers and digital signal processing (DSP), research has focused on 400Gb/s and 1Tb/s systems. To implement such systems, the use of multiple optical carriers is a viable solution to moderate the required increase in electrical bandwidth. In this scenario, tight channel spacing is required to achieve higher spectral efficiency (SE), however it is limited by linear crosstalk between adjacent channels. To overcome this, Nyquist pulse shaping as well as various types of multi-channel equalization (MCE) techniques have been considered [1]-[5]. The former is a widespread technique to transmit *sinc*-shaped pulses with a corresponding rectangular spectrum in order to minimize linear crosstalk. The latter consists of applying a multi-channel equalizer at the receiver to compensate for crosstalk. Several MCE techniques have been proposed such as the adaptive equalizer with least mean square algorithm, maximum *a posteriori* detection (MAP) [1], and FD-MIMO detection [2]-[5]. FD-MIMO generalizes the conventional constant modulus algorithm (CMA) used to separate dual polarization signals by also demultiplexing different carrier frequencies.

In addition to supporting commercially available compact external cavity lasers (ECL) for each optical carrier at the transmitter side, realistic values for the carrier frequency stability must also be taken into account in Nyquist or quasi-Nyquist spaced WDM systems. For example, the integrable tunable laser assembly multisource agreement (ITLA MSA), defined by the optical internetworking forum (OIF), outlines the specification for lifetime laser frequency drift. A frequency variation of ±1.25GHz and ±2.5GHz are defined for the 25GHz and 50GHz ITU grids, respectively. Therefore, the channel spacing may vary by a few GHz due to the ambient temperature deviation and aging over a long period of time, resulting in partial channel overlap. Rather than use Nyquist pulse shaping at the transmitter to avoid linear crosstalk, FD-MIMO adaptively compensates the crosstalk induced by this spectral overlap at the receiver, and thus, removes the stringent requirements on the filtering or carrier frequency stability. This technique has already been demonstrated for dual-polarization quadrature phase shift keying (DP-QPSK) in both numerical simulation [2] and experimental back-to-back measurements [3], [4].

Furthermore, sub-Nyquist channel spacing is attractive to increase the SE. However, a sub-Nyquist channel spacing will lead to an increase in linear crosstalk; inversely proportional to the channel spacing reduction. To realize sub-Nyquist spacing, a super-Nyquist approach, also known as faster-than-Nyquist, has been proposed [6]. The super-Nyquist signal is based on spectral shaping of the signal at the transmitter side and signal demodulation based on MAP or maximum likelihood sequence estimation on the receiver side. FD-MIMO detection has also been demonstrated for sub-Nyquist channel spacing [3], [4].

The generation and detection of channels with sub-Nyquist channel spacing has also been considered for frequency domain modulation formats. For example, a MAP receiver has been used to enable spectrally efficient frequency division

This work was supported by the U.K. EPSRC Programme Grant UNLOC (UNLocking the Capacity of Optical Communications) EP/J017582/1.

M. Sato is with Converged Network Division, NEC Corporation, 1131 Hinode, Abiko-shi, Chiba 270-1198, Japan (e-mail: m-satou@kj.jp.nec.com). The work was performed when he was a research visitor in the Optical Networks Group, Department of Electronic and Electrical Engineering, University College London, London WC1E 7JE, U.K.

R. Maher, D. Lavery, K. Shi, B. C. Thomsen, and P. Bayvel are with the Optical Networks Group, Department of Electronic and Electrical Engineering, University College London, London WC1E 7JE, U.K. (e-mail: r.maher@ucl.ac.uk; d.lavery@ee.ucl.ac.uk; k.shi@ucl.ac.uk; b.thomsen@ucl.ac.uk; p.bayvel@ucl.ac.uk).

Copyright (c) 2013 IEEE

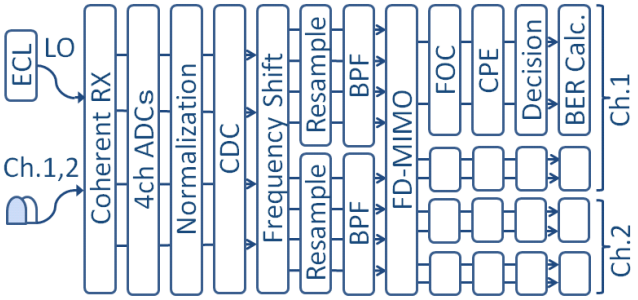

Fig. 1. Receiver configuration for the dual-carrier signal. ECL: external cavity laser; RX: receiver; ADCs: analog to digital converters; CDC: chromatic dispersion compensation; BPF: bandpass filter; FD-MIMO: frequency diversity multiple-input-multiple-output adaptive filter; FOC: frequency offset compensation; CPE: carrier phase estimation; BER: bit error rate.

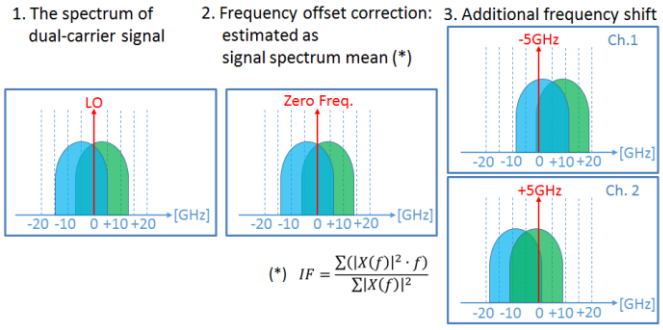

Fig. 2. An example of frequency shift block for 8GHz spaced dual-carrier 10GBaud DP-16QAM signal. This diagram only illustrates the x-polarization signal.

multiplexing (SEFDM), with an increased spectral efficiency of 25% [7]. Finally, we note that recent research has shown theoretically that joint coding of carriers with overlapping spectra can be used to mitigate linear crosstalk, and increase the achievable rate [8].

In our previous work [5], we experimentally demonstrated the transmission of a dual-carrier 10GBaud DP 16-*ary* quadrature amplitude modulation (16QAM) signal. The channel spacing was varied from 80% to 100% of the symbol rate and FD-MIMO was used to mitigate linear crosstalk. A small Q^2-factor penalty of 1.7dB was achieved with respect to single carrier performance after 800km transmission over SSMF.

In this paper, we experimentally investigate the optimum number of taps for the FD-MIMO equalizer and compare the performance to a Nyquist pulse shaped dual-carrier system after 800km transmission of SSMF. In the back-to-back configuration, the linear crosstalk mitigation of the dual-carrier DP-QPSK and DP-16QAM signals is demonstrated by varying the channel spacing from 40% to 120% of the symbol rate. Furthermore, optical spectral filtering is employed to constrain the bandwidth of the dual-carrier signal in order to suppress the sidelobes of the non-return-to-zero (NRZ) spectrum. The performance of FD-MIMO detection is subsequently analyzed by varying the bandwidth of the optical tunable filter at the transmitter. In addition, the applicability of FD-MIMO detection for a 3-channel WDM system is demonstrated. The influence of laser phase noise on the performance of FD-MIMO is also investigated through numerical simulations. Finally, the computation complexity of FD-MIMO is compared with Nyquist pulse shaping.

The remainder of this paper is organized as follows. In Section II, the receiver architecture used for this work is described. The experimental setup is introduced in Section III, while dual-carrier DP-16QAM transmission results, compared with Nyquist spectral pulse shaping, are presented in Section IV. Further experimental results for FD-MIMO in the back-to-back configuration are detailed in Section V. Section VI concludes this paper.

II. Receiver Architecture

The schematic of the receiver used in this work is shown in Fig. 1. The dual-carrier (channel) signal is initially converted to the electrical domain by the coherent receiver. The local oscillator (LO) wavelength is set approximately to the central frequency of the dual-carrier signal. The electrical signal is then sampled by a 4-channel ADC, and skew compensation and normalization are applied. Then, chromatic dispersion compensation (CDC) is jointly applied in the frequency domain for the two carriers [9]. Next, the dual-carrier signal is centered at the zero frequency by applying a frequency offset correction, which is estimated as the mean frequency of the entire signal spectrum. Once the dual-carrier signal is centered around baseband, each individual carrier is down converted separately by applying an additional frequency shift of ± half the symbol rate, as shown in Fig. 2. Subsequently, each channel is resampled to 2 Sa/Sym, and a bandpass filter is applied immediately before the FD-MIMO equalization.

For the dual-carrier signal, a 4x4 MIMO adaptive equalizer is used to recover the two polarization states on each channel. For the DP-16QAM signal, equalizer pre-convergence is achieved using the CMA before switching to radially directed equalization (RDE), whereas QPSK uses a standard CMA equalizer [10]. The equalized signal, per polarization/channel, is then separately processed for frequency offset (FO) compensation, carrier phase estimation (CPE) and symbol hard decisions. The FO estimator uses a 4^{th}–order non-linearity algorithm, while the CPE uses decision-directed phase estimation [11]. Finally BER estimation is performed for each channel.

For the 3-channel system, the receiver architecture is slightly modified from the dual-carrier case. The LO laser wavelength is set to the central channel and a frequency shift of ± the symbol rate is applied for each neighboring channel. This down converted each individual channel before being passed to a 6x6 MIMO adaptive equalizer.

Note that an alternative receiver configuration using multi-coherent RX was proposed in [2]. It is possible to relax the required bandwidth of the coherent RX and ADC, however the theoretical studies have showed that it also requires a frequency-locked LO comb [2].

III. Experimental Setup

Fig. 3 shows the experimental configuration used in this work.

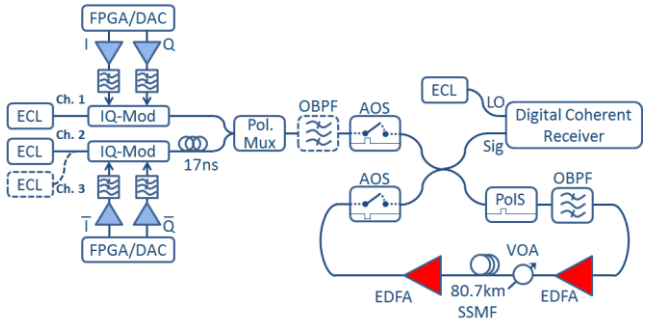

Fig. 3. Experimental configuration. IQ-Mod: IQ modulator; FPGA: field programmable gate array; DAC: digital to analog converter; Pol.Mux: polarization multiplexer; OBPF: optical bandpass filter; AOS: acousto-optic switch; PolS: polarization scrambler; EDFA: Erbium doped fiber amplifier; VOA: variable optical attenuator; SSMF: standard single mode fiber.

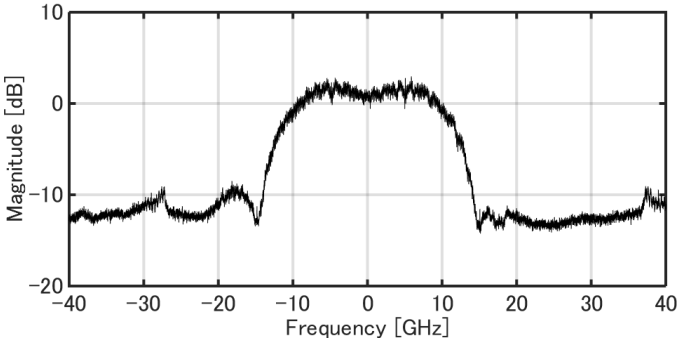

Fig. 4. The spectrum of the coherently detected 10GHz spaced dual-carrier DP-16QAM signal (20MHz resolution).

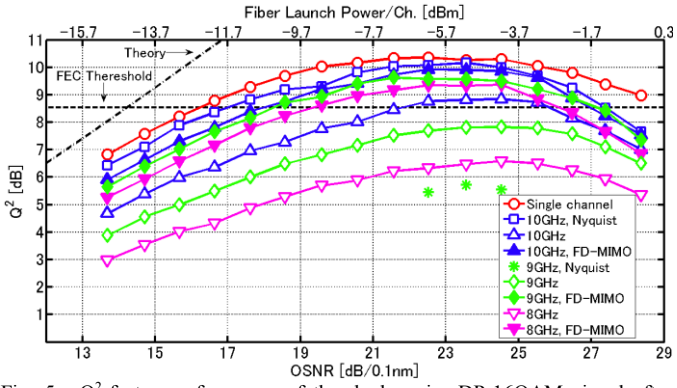

Fig. 5. Q^2-factor performance of the dual-carrier DP-16QAM signal after transmission over 807km SSMF.

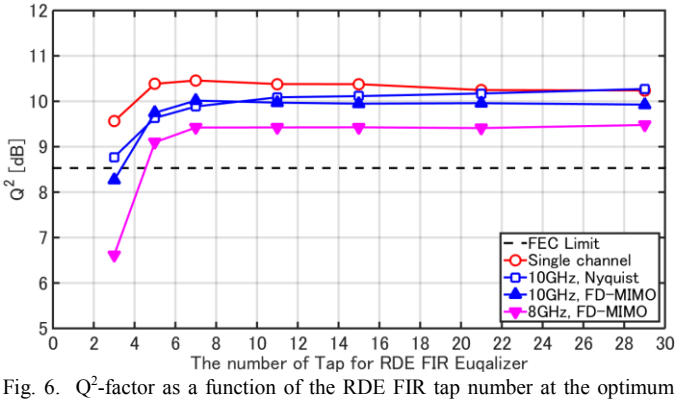

Fig. 6. Q^2-factor as a function of the RDE FIR tap number at the optimum launch power after transmission over 807km of SSMF. RDE: radially directed equalization; FIR: finite impulse response

Two ECLs, each with a 100kHz linewidth were individually modulated by two IQ modulators. Ch.1 was set at 1550nm, while the frequency of Ch. 2 was adjusted between +4GHz and +12GHz from Ch.1. An additional ECL was used for the three channel case, and was bulk modulated with Ch.2. In this case, Ch.2 and Ch.3 were located between ±8GHz and ±12GHz from Ch.1. A set of four de-correlated pseudo random binary sequences (PRBS) of length 2^{15}-1 were digitally generated, mapped onto 16QAM symbols and stored on a field-programmable gate array (FPGA). DP-QPSK used a set of two de-correlated 2^{15}-1 PRBSs. The 10GBaud in-phase (I) and quadrature (Q) signals were generated by Micram digital to analog converters (DAC) at a sample rate of 20GS/s. An electrical linear amplifier was used to ensure a sufficient voltage level for the IQ modulator and a 5th-order electrical Bessel low pass filter (LPF), with a cut-off frequency of 7GHz, was applied for the image reduction. In the case of Nyquist pulse shaping, the transmitted sequence was shaped by a root-raised-cosine (RRC) 128 tap filter with a roll-off factor of 0.1% and cascaded 8th-order electrical LPFs with cut-off frequencies of 5.5GHz and 7GHz LPF were used for the image rejection. The two WDM channels were de-correlated by 170 symbols before the polarization multiplexing emulation stage (Pol. Mux.). Note that the optical power for of each channel was carefully equalized (< 0.5dB variation) and maintained constant at this value throughout the experiment. In the back-to-back analysis, the Pol. Mux. was connected to the signal port of the coherent receiver and an amplified spontaneous emission (ASE) noise loading stage was used for optical signal-to-noise ratio (OSNR) adjustment. A Kylia XTM-50 Ultrafine tunable optical bandpass filter (OBPF) was inserted after the Pol. Mux for the optical spectral filtering experiment.

In transmission, a single-span optical fiber recirculating loop was used. The loop consisted of two acousto-optic switches (AOS), two Erbium doped fiber amplifiers (EDFAs), a polarization scrambler, OBPF to reject out of band ASE, and 80.7km of SSMF with an attenuation coefficient of 0.19dB/km and a dispersion parameter of 17ps/(nm.km).

The coherent receiver consisted of a discrete dual-polarization 90˚ optical hybrid, four balanced photo detectors with 70GHz electrical bandwidth and a four channel real time sampling oscilloscope with a sample rate of 160GS/s and an electrical bandwidth of 63GHz. An ECL with a 100kHz linewidth was used as the LO and the emission frequency was set to +5GHz from Ch.1 to capture the complete dual-carrier signal for offline signal processing, as described above. The LO was set at the center of Ch.1 (1550nm) for the three-channel experiments. Note that the length of the RDE finite impulse response (FIR) filters was set to 21 taps (T/2 spaced), and a 64 tap T-spaced sliding window was applied for CPE. The single channel case used a standard 2x2 CMA configuration, with subsequent DSP operating on a single channel only. For the dual-carrier signal without FD-MIMO, the frequency shift used to detect the target channel was applied prior to resampling. In addition, matched Nyquist filtering was applied after CDC for the Nyquist pulse shaped transmitter.

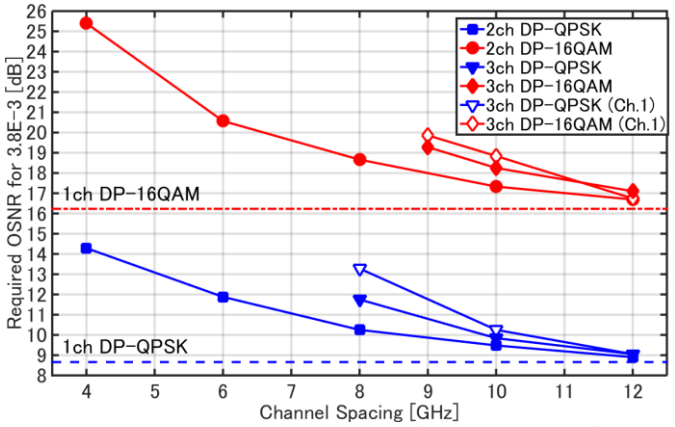

Fig. 7. Performance of FD-MIMO detection in the back-to-back configuration. Required OSNR to achieve a BER of $3.8\text{x}10^{-3}$ (Q^2-factor of 8.53dB) as a function of channel spacing with different transmitted signals.

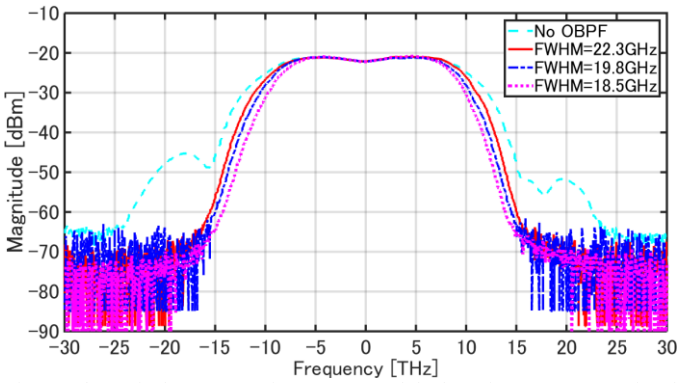

Fig. 8. The optical spectrum of 10GHz spaced dual-carrier DP-16QAM signal with different filter bandwidth settings for the optical tunable filter. FWHM: full width at half maximum.

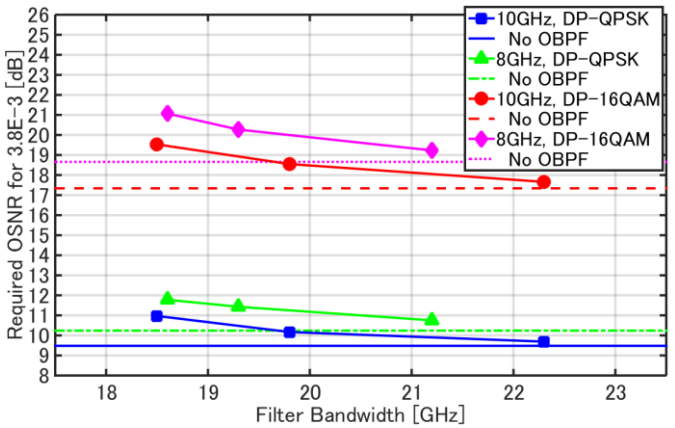

Fig. 9. The filtering tolerance for the dual-carrier DP-16QAM / DP-QPSK signal with 10GHz and 8GHz channel spacings. The required OSNR to achieve a BER of $3.8\text{x}10^{-3}$ (Q^2-factor of 8.53dB) as a function of filter bandwidth.

Fig. 4 shows the spectrum of the coherently detected 10GHz spaced dual-carrier DP-16QAM signal. The variation in the spectral sidelobes for each subcarrier was a result of the different frequency responses of each electrical Bessel LPF used in the experiment.

IV. Dual-carrier DP-16QAM transmission results

In Fig. 5, the Q^2-factor of the three formats is plotted as a function of both the received OSNR and the fiber launch power after transmission over 807km of SSMF and for three channel spacings (8GHz, 9GHz, and 10GHz). The Q^2-factor was derived from the average measured bit error rate (BER), over the two polarizations and the two channels. An implementation penalty of 1.7dB for the single channel case was measured at the forward error correction (FEC) threshold BER value of 3.8×10-3 (or the equivalent Q2-factor of 8.53dB) in the back-to-back configuration. Further details of the back-to-back experimental configuration and results are described in [5]. From Fig. 5, it is evident that without FD-MIMO, the dual-carrier signal (spaced at 10GHz) suffered from strong crosstalk as it showed a maximum penalty of 2dB in Q^2-factor from the single channel case. Decreasing the channel spacing to 8GHz resulted in a 3.5dB penalty in the linear region at launch powers below -9dBm, where the penalty is dominated by the accumulated ASE noise of the EDFAs. Under the same conditions, applying FD-MIMO processing significantly improved performance. The Q^2-factor penalty was only 0.7dB with a 10GHz channel spacing, increasing to 1.7dB as the channel spacing was reduced to 8GHz. These results confirm that FD-MIMO effectively mitigates linear crosstalk from the neighboring channel, even if the channel spacing were to fluctuate significantly by ±2GHz. As the fiber launch power increased, the effectiveness of FD-MIMO is reduced due to nonlinear fiber distortions.

Fig. 5 also illustrates the performance of the system when Nyquist pulse shaping was employed at the transmitter which also used the conventional 2x2 MIMO (10GHz channel spaced dual-carrier signal). Compared to the Nyquist pulse shaped dual-carrier signal, the FD-MIMO showed a Q^2-factor penalty of less than 0.6dB. A smaller penalty was observed as a function of increased launch power for the non-return-to-zero format as it is more tolerant to fiber nonlinearities than the Nyquist pulse shaped signal. Note that at the optimum launch power of -5dBm for both scenarios, the relative Q^2-factor penalty for FD-MIMO is only 0.25dB. In addition, the Nyquist pulse shaped dual-carrier signal with sub-Nyquist channel spacing exhibited poor tolerance to linear crosstalk. The 9GHz spaced Nyquist pulse shaped dual-carrier DP-16QAM signal suffered from strong crosstalk and with the resultant Q^2-factor of 5.7dB at the optimum launch power of -5dBm. Moreover, applying FD-MIMO processing proposed here to the sub-Nyquist spaced (9GHz spacing) 10Gbaud Nyquist signal was ineffective in improving the performance. To improve the performance of a sub-Nyquist system such as this, a maximum likelihood detector is required [12].

Fig. 6 shows the Q^2-factor versus the number of RDE FIR filter taps at the optimum launch power after 807km of SSMF. Tap numbers greater than 7 were sufficient for FD-MIMO, which is similar to the single channel case. The performance of the Nyquist pulse shaped dual-carrier signal improved as the number of taps increased and this is due to the longer impulse response associated with Nyquist pulse shaping. Therefore, 21 taps is sufficient to perform and accurate comparison between FD-MIMO and Nyquist pulse shaping.

V. BACK-TO-BACK ANALYSIS FOR FD-MIMO

Firstly, we investigated the linear crosstalk mitigation performance of the FD-MIMO technique under various conditions, such as channel spacing, modulation format, and the number of channels. In Fig. 7, the required OSNR to achieve Q^2-factor of 8.53dB (corresponding to a 7% HD-FEC threshold) is plotted as a function of channel spacing, and compared with four different configurations; dual-carrier DP-QPSK and DP-16QAM, and 3-channel DP-QPSK and DP-16QAM. Note that all formats used FD-MIMO except the single channel cases. As before, the Q^2-factor was derived from the average BER over the two polarizations and all channels. To analyze the worst case scenario, the Q^2-factor for the central channel (Ch. 1) for the 3-channel case is also plotted. It can be seen from Fig. 7 that the required OSNR increased as the channel spacing was reduced. The penalty for 16QAM increased faster than QPSK due to the lower tolerance for linear crosstalk. In the dual-carrier scenario, both modulation formats could be transmitted with a channel spacing as low as 4GHz, provided that the additional implementation penalties of 5.6dB and 9.1dB relative to single channel performance, could be tolerated for the DP-QPSK and DP-16QAM systems respectively. From a practical perspective, we note that the channel spacing could be reduced to 6.3GHz for QPSK, and 7.4GHz for 16QAM with a 3dB penalty.

The three channel system suffered more from linear crosstalk than the dual-carrier signal. As shown in Fig. 7, the OSNR penalty was 3dB higher compared to the single channel case, when the channel spacing was reduced to 8GHz for QPSK and 9GHz for 16QAM. The decrease in performance is due to the fact that the linear crosstalk for the central channel (affected by two neighbors) is more significant than the two outer channels (one neighbor only). The central channel performance was 1.5dB worse than the average results, when the channel spacing was 8GHz for QPSK, and 9GHz for 16QAM. The Q^2-factor of the central channel was 7.25dB for the 12GHz spaced 3-channel DP-16QAM signal using the conventional 2x2 MIMO without ASE Noise loading. The FD-MIMO equalizer improved the received Q^2-factor to 12.6dB. These results indicate that the performance is limited by the central channel for channel spacings less than the Nyquist frequency, even though FD-MIMO significantly mitigates linear crosstalk. Note that the outer carriers could also incur linear crosstalk on the central carrier when the number of channels is greater than 4. Considering the 6x6 MIMO equalizer which would be used in a 5-channel WDM system, the crosstalk from the outer carriers can be treated as random noise, so it may slightly degrade the performance [2].

Next, the optical spectral filtering for the dual-carrier signal with FD-MIMO is analyzed. Considering a Nyquist or quasi-Nyquist spaced WDM system, linear crosstalk comes from the adjacent channels. By using the 3-channel FD-MIMO equalization, the linear crosstalk from both neighboring channels can be mitigated. However, it requires more hardware and computational complexity, compared to the dual-carrier case.

The complexity of the FD-MIMO receiver is determined by the number of complex multiplications per symbol per channel that the bandpass filter (BPF), used to provide frequency diversity, and the MIMO equalizer require. For M interfering carriers M BPF are required and each BPF of L taps has complexity L, so that the total complexity of the BPF is L per symbol per channel. A MxM MIMO equalizer with N T/2 fractional-spaced taps requires MN multiplications for output calculation, and MN+1 multiplications for the update of the coefficients. Therefore, the computational complexity of the time domain implementation of the FD receiver can be expressed as:

$$C_{FD} = L + 2MN + 1 \qquad (1)$$

Table 1 shows the computational complexity of FD receiver per channel. The BPF required L=16 taps and the MIMO equalizer required N=7 taps, values selected as sufficient for FD-MIMO according to the experimental results in Fig. 6.

In the Nyquist system each channel must be filtered at the transmitter and then the corresponding matched filter applied at the receiver. In order to achieve minimal crosstalk between the two Nyquist spaced subcarriers it is necessary to employ a Nyquist pulse shaping filter with approximately L=128 taps [13]. Thus the system complexity of Nyquist pulse shaping is $C_N = 2L + 4N + 1$ per symbol per channel.

Table 1. The computational complexity (number of complex multiplications) of FD receiver per channel with L=16 and N=7 filter taps, compared to the Nyquist System with L=128.

M	*2*	*4*	*6*
C_{FD}	45	73	101
C_N	264	264	264

Table 1 showed even though FD-MIMO complexity linearly increased as a function of channel number, it is significantly lower than the complexity of the Nyquist system for up to 3 carriers. However, the DSP implementation for multi-channel signal processing in ASIC is challenging, either using a single chip or using multiple synchronized chips. Once the semiconductor processes improve to realize large scale ASICs for multi-channel signal processing, the complexity of FD-MIMO would not be prohibitive.

Therefore, a dual-carrier signal with a sufficient guard band could be employed as an alternative to 3-channel FD-MIMO detection to avoid the crosstalk from other carriers in WDM system. Compared with ideal Nyquist pulse shaping, the NRZ signal has twice the bandwidth due to the sidelobes of the spectrum. Considering the ideal Nyquist pulse shaped dual-carrier signal, it requires a 2×symbol-rate channel spacing in a WDM system, whereas the NRZ shaped dual–carrier signal requires an additional 1×symbol-rate guard band to avoid linear crosstalk. Therefore, one must reduce the guard band to increase the SE in this scenario. In our experiments, we used a tunable OBPF at the transmitter and varied the optical filter bandwidth to suppress the sidelobes of the NRZ spectrum, thereby reducing the channel guard band. Note that the filtering method is not limited to the tunable OBPF, it is also possible to use an arrayed-waveguide grating for this purpose, as

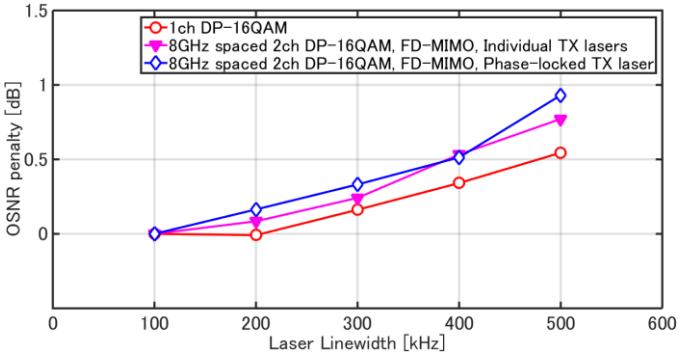

Fig. 10. The laser linewidth tolerance for the dual-carrier DP-16QAM with 8GHz channel spacing. The OSNR penalty at the FEC threshold (Q^2-factor of 8.53dB) is plotted versus laser linewidth for three different cases.

commonly used in WDM systems.

Fig. 8 shows the optical spectrum of the 10GHz spaced dual-carrier DP-16QAM signal with varying filter bandwidth. The data was captured using an optical spectrum analyzer with 0.01nm resolution. The sharp roll-off of the optical filter can be observed from Fig. 8, and the sidelobes of the dual-carrier signal are eliminated by the filter. Fig. 9 illustrates the filtering tolerance for the dual-carrier DP-QPSK and DP-16QAM signal with 10GHz and 8GHz channel spacing. The required OSNR to achieve a Q^2-factor of 8.53dB as a function of the filter bandwidth (full width half maximum) is displayed. Generally, the penalty with respect to having no OBPF gradually rose as the filter bandwidth was decreased below approximately 20GHz. A similar trend was observed with the linear crosstalk case in Fig. 7 (16QAM showed a lower tolerance to filtering than QPSK). A channel spacing of 10GHz demonstrated a similar tolerance to the 8GHz spaced dual-carrier signal. Therefore, an additional penalty of 0.5dB allowed a reduction in the optical filter bandwidth to 22GHz, providing a SE comparable to the Nyquist spaced WDM system with a 10% margin.

Finally, the influence of laser phase noise (originating from the transmitter laser and the LO) on the performance of FD-MIMO was investigated through numerical simulations. Experimental constraints were also included in the simulation, such as introducing additive white Gaussian noise at the transmitter and including the effective number of bits (ENOB) of the DAC (measured ENOB of 3.2 at 10GHz). The OSNR penalty at the FEC threshold (Q^2-factor of 8.53dB), as a function of laser noise, is shown in Fig. 10 for an 8GHz spaced dual-carrier DP-16QAM signal and a single channel case. FD-MIMO processing was used in the receiver and two scenarios were investigated; firstly when two independent lasers were used in the transmitter and secondly when a phase locked two-channel laser was used.

When independent lasers were used at the transmitter, the OSNR penalty increased, with a corresponding increase in phase noise, and resulted in an additional penalty of 0.8dB for a laser linewidth of 500kHz, only 0.3dB greater than in the single channel case. The cycle slips were present at laser linewidths greater than 600kHz for both cases, due to that CPE failing when $\Delta\nu T_s$ exceeded a value of approximately 1E-4, where $\Delta\nu$ is the combined linewidth of the transmitter laser and the LO [11]. Different from the other algorithms, for example the decision directed least mean square algorithm, RDE does not use the signal phase to update the MIMO equalizer. Therefore, an increase of the phase noise simply introduced a constant penalty. The performance of the FD-MIMO system did not improve when a phase-locked laser was used in the transmitter, regardless of the increase in phase noise. The required OSNR for the FEC threshold was also same as the case using independent lasers with a laser linewidth of 100kHz. It might be possible to improve the performance combined with the joint carrier phase estimation technique, but this will be investigated in future research.

In addition, since 100kHz linewidth ECLs are commonly used in commercial WDM systems, it can be assumed that FD-MIMO demonstrated a sufficient level of robustness to moderate values of phase noise associated with these sources.

VI. Conclusion

In this paper, we experimentally demonstrated dual-carrier 10GBaud DP-16QAM transmission using FD-MIMO. FD-MIMO was shown to be effective in significantly mitigating linear crosstalk, even in the presence of finite frequency instability of the transmitter lasers. A maximum Q^2-factor penalty of less than 1.7dB was observed relative to the single channel case after more than 800km transmission. Also, the required number of filter taps for FD-MIMO was studied, and showed a similar trend to the single channel case.

FD-MIMO detection with sub-Nyquist channel spacing was investigated in a back-to-back configuration and the channel spacing was reduced to as low as 4GHz. If a 3dB penalty can be accepted, FD-MIMO enabled a channel spacing of 6.3GHz for QPSK, and 7.4GHz for 16QAM. The 3-channel FD-MIMO equalization was studied in the same configuration. Although the central channel suffered from stronger crosstalk, Nyquist spaced transmission was demonstrated with a OSNR penalty below 3dB. Additionally, the combination of optical filtering and FD-MIMO was experimentally studied in the dual-carrier WDM transmission. A Nyquist spaced WDM system with 10% margin was realized for both modulation formats with an additional penalty of 0.5dB.

These results show that FD-MIMO is a promising technique to counteract limitations in frequency stability of transmitter lasers to enable transmission of Nyquist spaced WDM channels without Nyquist pulse shaping,

Acknowledgment

The support under the UK EPSRC Programme Grant UNLOC (UNLocking the capacity of Optical Communications) EP/J017582/1 is gratefully acknowledged.

References

[1] J. Pan, C. Liu, T. Detwiler, A. J. Stark, Y. Hsueh, and S. E. Ralph, "Inter-Channel Crosstalk Cancellation for Nyquist-WDM Superchannel Applications," *J. Lightw. Technol.*, vol. 30, no. 24, pp. 3993-3999, Dec. 2012.

[2] T. Zeng, "Superchannel transmission system based on multi-channel equalization," *Opt. Exp.*, vol. 21, no. 12, pp. 14799-14807, Jun. 2013.
[3] N. Kaneda, T. Pfau, and J. Lee, "Frequency Diversity MIMO Detection for Coherent Optical Transmission," in *Proc. ECOC*, Sep. 2013, paper. Th.2.C.1.
[4] N. Kaneda, T. Pfau, and J. Lee, "Frequency Diversity MIMO Detection in Polarization Multiplexed Coherent Optical Transmission," in *Proc. OECC*, Jul. 2014, pp. 1051-1052.
[5] M. Sato, R. Maher, D. Lavery, K. Shi, B. C. Thomse, and P. Bayvel, "Frequency Diversity MIMO Detection for Dual Carrier DP-16QAM Transmission," in *Proc. ECOC*, Sep. 2014, paper. Th.2.5.1.
[6] J. Zhang, J. Yu, Z. Jia, and H. Chien, "400 G Transmission of Super-Nyquist-Filtered Signal Based on Single-Carrier 110-GBaud PDM QPSK With 100-GHz Grid," *J. Lightw. Technol.*, vol. 32, no. 19, pp. 3239-3246, Oct. 2014.
[7] I. Darwazeh, T. Gui, Y.Bao, and Z. Li, "Optical SEFDM System; Bandwidth Saving Using Non-Orthogonal Sub-Carriers," *IEEE Photon. Technol. Lett.,* ,vol. 26, no. 4, pp. 352-355, Feb. 2014.
[8] T. Koike-Akino, K. Kojima, D. S. Millar, K. Parsons, S. Kametani, T. Sugihara, T. Yoshida, K. Ishida, Y. Miyata, W. Matsumoto, and T. Mizuochi, "Interference Management with Han-Kobayashi Coding: Dual-Carrier Coherent Optical Communications," in *Proc. ECOC,* Sep. 2014, paper. Mo.3.5.1.
[9] E. Ip and J. M. Kahn, "Digital Equalization of Chromatic Dispersion and Polarization Mode Dispersion," *J. Lightw. Technol.*, vol. 25, no. 8, pp. 2033-2043, Aug, 2007.
[10] M.J. Ready and R. P. Gooch, "Blind equalization based on radius directed adaptation," *ICASSP*, vol. 3, pp. 1699-1702, April, 1990.
[11] I. Fatadin, D. Ives, and S. J. Savory, "Blind equalization and Carrier Phase Recovery in a 16-QAM Optical Coherent System," *J. Lightw. Technol.*, vol. 27, no. 15, pp. 3042-3049, Aug, 2009.
[12] J. Cai, Davidson, C. R. Davidson, A. Lucero, H. Zhang, D. G. Foursa, O. V. Sinkin, W. W. Patterson, A. N. Pilipetskii, G. Mohs, and N. S. Bergano, "20 Tbit/s Transmission Over 6860 km With Sub-Nyquist Channel Spacing, "*J. Lightw. Technol.*, vol. 30, no. 4, pp. 651-657, Feb, 2012.
[13] R. Maher, M. Sato, T. Xu, L. Galdino, S. Kilmurray, S. J. Savory, B.C. Thomsen, R. Killey, P. Bayvel, "Digital pulse shaping to mitigate linear crosstalk in Nyquist-spaced 16QAM WDM transmission systems," in *Proc. OECC / ACOFT,* Jul. 2014, paper. MO2B-2.

Masaki Sato received the M.E. degree in Information Systems Science from the University of Electro-Communications, Tokyo, Japan, in 2005.

In 2005, he joined NEC Corporation, Abiko, Japan, where he was involved in development of long-haul WDM transmission systems. In September 2013, he joined the Optical Networks Group, University College London as a visiting researcher for 12 months. He is currently with Converged Network Division, NEC Corporation.

Robert Maher's biography appears in a literature:
D. Lavery, R. Maher, D. S. Millar, B. C. Tomsen, P. Bayvel, and S. J. Savory, "Digital Coherent Receivers for Long-Reach Optical Access Networks," *J. Lightw. Technol.*, vol. 31, no. 4, pp. 609-620, Feb, 2013.
Available: http://dx.doi.org/10.1109/JLT.2012.2224847

Domaniç Lavery's biography appears in the literature:
D. Lavery, R. Maher, D. S. Millar, B. C. Tomsen, P. Bayvel, and S. J. Savory, "Digital Coherent Receivers for Long-Reach Optical Access Networks," *J. Lightw. Technol.*, vol. 31, no. 4, pp. 609-620, Feb, 2013.
Available: http://dx.doi.org/10.1109/JLT.2012.2224847

Kai Shi (M'12) received the BSc degree in optical information science and technology, the MEng degree in optoelectronics information engineering, from the Huazhong University of Science and Technology, Wuhan, China, in 2006 and 2008 respectively, and the PhD degree from Dublin City University (DCU), Ireland, in 2012.

From 2012 he worked as a Research Assistant at the Rince Institute, DCU. His research at DCU involved the characterisation and application of wavelength-tunable lasers for dynamic optical networks. Since October 2012, he has been a Research Associate with the Optical Networks Group (ONG) at University College London (UCL). His research interests include technologies and systems required to exploit the spatial dimension of multimode optical fibre using coherent optical reception.

Benn C. Thomsen's biography appears in the literature:
D. Lavery, R. Maher, D. S. Millar, B. C. Tomsen, P. Bayvel, and S. J. Savory, "Digital Coherent Receivers for Long-Reach Optical Access Networks," *J. Lightw. Technol.*, vol. 31, no. 4, pp. 609-620, Feb, 2013.
Available: http://dx.doi.org/10.1109/JLT.2012.2224847

Polina Bayvel's biography appears in the literature:
D. Lavery, R. Maher, D. S. Millar, B. C. Tomsen, P. Bayvel, and S. J. Savory, "Digital Coherent Receivers for Long-Reach Optical Access Networks," *J. Lightw. Technol.*, vol. 31, no. 4, pp. 609-620, Feb, 2013.
Available: http://dx.doi.org/10.1109/JLT.2012.2224847